Applied Catalysis B: Environmental 212 (2017) 159–174

Contents lists available at ScienceDirect

Applied Catalysis B: Environmental

journal homepage: www.elsevier.com/locate/apcatb

Research paper

Ni/CeO_2 based catalysts as oxygen vectors for the chemical looping dry reforming of methane for syngas production

Axel Löfberg*, Jesús Guerrero-Caballero, Tanushree Kane, Annick Rubbens, Louise Jalowiecki-Duhamel*

Univ. Lille, CNRS, Centrale Lille, ENSCL, Univ. Artois, UMR 8181, UCCS, Unité de Catalyse et Chimie du Solide, F-59000 Lille, France

ARTICLE INFO

Article history:
Received 6 February 2017
Received in revised form 8 April 2017
Accepted 18 April 2017
Available online 22 April 2017

Keywords:
Dry reforming of methane
Chemical looping
Nickel
Ceria

ABSTRACT

Chemical looping dry reforming of methane (CLDRM) is performed by exposing a Ni/CeO_2 solid to CH_4 and CO_2 in a cyclic way. The solid acts as an oxygen vector producing syngas ($CO + H_2$) during exposure to CH_4, and is re-oxidized during exposure to CO_2. Absence of CO_2 during syngas production allows suppressing reverse water gas shift reaction and reaching high selectivity. Exposure to CO_2 restores the oxygen capacity of the support and removes residual carbon formed at the surface, thus fully regenerating the catalyst. Solids were characterized by TPR, XRD, Raman scattering, and XPS. Results show that part of the Ni is reduced and remain in metallic state during the looping process. On the other hand, Ni^{2+} species in strong interaction with Ce cations are observed even after exposure to methane. Both Ni species play important roles on reactants activation and oxygen supply by the solid. Ni loading is a crucial parameter for controlling the reduction behavior of the support and therefore for CLDRM process optimization.

1. Introduction

The valorization of methane into liquid fuels or high hydrocarbons has attracted renewed attention in the last years [1] due to two main factors, the large volume of methane resources available as compared to petroleum, particularly since the exploitation of shale gas has been developed [2,3], and the remarkable contribution to the greenhouse effect of this molecule.

Combining the valorization of CH_4 with that of CO_2 through the dry reforming of methane (DRM, Eq. (I)) brings the advantage of consuming another gas which contributes strongly to the global warming. DRM produces H_2 and CO, which jointly or separately, are the raw materials for different processes producing energy and chemicals, e.g. through Fischer-Tropsch synthesis.

$$CH_4 + CO_2 \rightarrow 2H_2 + 2CO \quad \Delta H^\circ = 247\,kJ/mol \tag{I}$$

Among the difficulties is the formation of coke due to the decomposition of methane into carbon and hydrogen (Eq. (II)) [4] or by the disproportionation of carbon monoxide (Boudouard reaction, Eq. (III)) [5] at the high operating temperatures. In both cases, this leads to the formation of carbon and to the probable deactivation of the catalyst. Sintering of the active species at the high temperatures needed to perform such reaction is another cause of catalysts deactivation.

$$CH_4 \rightarrow C + 2H_2 \quad \Delta H^\circ = 75\,kJ/mol \tag{II}$$

$$2CO \rightarrow C + CO_2 \quad \Delta H^\circ = -171\,kJ/mol \tag{III}$$

Another drawback of DRM is due to the simultaneous presence of CO_2 (reactant) and hydrogen (product) leading, by the reverse water gas shift (RWGS, Eq. (IV)) reaction, to a loss in selectivity.

$$CO_2 + H_2 \rightarrow CO + H_2O \quad \Delta H^\circ = -41\,kJ/mol \tag{IV}$$

One solution to overcome these drawbacks consists in separating the reactant and performing DRM in a so-called chemical looping process. It consists in reacting methane with an oxygen vector material that would get reduced and produce selectively syngas (Eq. (V)). In a second time, the reduced solid would be re-oxidized by CO_2 to regenerate the oxygen vector (Eq. (VI)). The process globally corresponds to the catalytic DRM although in practice it consists of two independent gas-solid reactions (Fig. 1).

$$CH_4 + Sol - O \rightarrow 2H_2 + CO + Sol - R \tag{V}$$

$$CO_2 + Sol - R \rightarrow Sol - O + CO \tag{VI}$$

$$Sol\text{-}O = oxidizedcatalystandSol\text{-}R = reducedcatalyst$$

Although the overall process would remain endothermic as in co-feed DRM, chemical looping would bring several advantages mainly in terms of catalysts deactivation and selectivity as, first,

* Corresponding authors.
E-mail addresses: Axel.Lofberg@univ-lille1.fr (A. Löfberg), Louise.Duhamel@univ-lille1.fr (L. Jalowiecki-Duhamel).

http://dx.doi.org/10.1016/j.apcatb.2017.04.048
0926-3373/

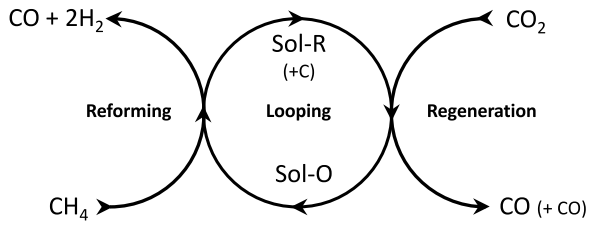

Fig. 1. Illustration of CLDRM process.

the deactivation by carbon is avoided as the solid is regenerated in each cycle and deposited carbon can be re-oxidized by CO_2 (reverse Eq. (III)). Second, the hydrogen produced in the first step is never in contact with the carbon dioxide, thus avoiding the RGWS (Eq. (IV)).

Several industrial techniques have been already applied since decades in order to improve reaction systems on this way [6–9]. The main difference from co-feed processes is the ability of decoupling the reaction in two. Therefore, the operation conditions can be optimized independently, obtaining in some cases improved performances in respect to that reached in co-feed.

To some extent this approach is similar to that proposed for the redox decoupling of Mars and Van Krevelen reactions, e.g. for butane selective oxidation to maleic anhydride [10,11]. It should be noted however that such mechanism has not been proved for DRM although Sadykov et al. have suggested it may apply in the case of fluorite and perovskite supported metal nanoparticles [12].

One of the first researchers to propose such system for DRM for syngas production was Otsuka et al. [13] in 1998 on Pt-CeO_2 based catalyst.

Bhavsar et al. [14–17] proposed a concept for the combustion of methane and the production of CO consisting of a variant of chemical looping combustion (CLC) using CO_2 instead of O_2. Although the production of hydrogen was not the goal, they defined the process as a "chemical looping dry reforming of methane". They essentially focused on Fe-CeO_2 systems which indeed do not lead to selective oxidation in syngas but to total combustion to CO_2 and water. CO is essentially produced during the regeneration step. They discussed about the relevance of the oxidation state of iron towards the selectivity of the products. The distribution goes from a total oxidation of CH_4 (from Fe_2O_3 to Fe_3O_4), going through a mix of total-partial oxidation to syngas (from Fe_3O_4 to FeO) and ending with the formation of carbon when the reduction of the solid is complete (Fe°). Even though the oxidation by CO_2 gives another "initial" state of Fe species (Fe_3O_4) for the next cycle, the system is still not 100% selective towards H_2 and CO. This will certainly depend on the nature of the oxygen vector but can also depend on the diffusion rate of oxygen which needs to be optimal for the partial oxidation. If the rate is too high the total oxidation of methane can take place producing H_2O and CO_2, on the contrary, if it is too slow carbon deposition can be produced from the decomposition of methane. Zhu et al. have also proposed the use of CeO_2-Fe_2O_3 materials as oxygen carriers for the steam reforming of ethane in chemical looping systems [18].

More recently, Galvita et al. [19] went further in such concept by proposing Ni promoted Fe-CeO_2 solids for the same application with relevant increases in performances but still aiming towards total oxidation and not syngas production. Similarly, Bhavsar studied NiFe-CeO_2 systems in a looping process mostly focusing on the oxidation step for CO_2 valorization to CO [17].

In the case of methane reforming for syngas production, the main challenges are (i) to obtain the partial oxidation of methane without neither CO_2 nor H_2O during the first step, (ii) possibly using transition metals-based catalysts and (iii) keeping a high activity towards methane while producing as little carbon deposition as possible. This last point is less crucial than the previous considering that eventual carbon deposits may be removed during the regeneration step. It can be worthy nevertheless to limit such carbon deposit as much as possible. Indeed, in another proposal for periodic reforming of methane with CO_2, S. Assabumrungrat et al. [20] suggested to use Ni/SiO_2-MgO based catalysts to perform the decomposition of methane in carbon and hydrogen in a first step and the combustion of this carbon by CO_2, producing CO, in a second. In this case, the solid does not act as an oxygen vector. Although the results were promising they showed that a certain amount of oxygen needed to be added in the CO_2 stream in order to achieve full removal of carbon.

Very recently, Tang et al. proposed a comprehensive review of the state of the art of chemical-looping process for reforming of methane [21], with a particular attention toward the oxygen vector materials. One of the key points is the possible re-oxidation by CO_2 instead of O_2.

CeO_2 is well known for its oxygen mobility and storage capacity. From the thermodynamic point of view, the oxidation of reduced ceria by CO_2 is favorable at 25 °C up to more than 1000 °C [20]. Otherwise, the main constrains come from the slow kinetics at low temperatures, even using noble metals to accelerate the process. Li et al. [22] attributed the activation of CO_2 on CeO_2 to the rapid formation of carbonates and carboxylates species on partially reduced CeO_{2-x}, which could remain on the surface of the solid up to 500 °C. However, some other studies concluded that CO_2 can be directly dissociated to CO and active oxygen species by the metal-ceria catalyst, donating oxygen to a lattice vacancy and producing CO, which is totally desorbed at around 450 °C [23,24]. In addition, Jin et al. [25] observed in a Temperature Programmed Desorption of CO_2 on Pt/CeO_2, the production of CO around 280 °C (the catalyst was pre-reduced under H_2). Moreover, Sharma et al. [26] noted that the oxidation of ceria by CO_2 was negligible in measurements using Pd/ceria at 200 °C, implying that indeed there are kinetic limitations to its oxidation by carbon dioxide. Nevertheless, they demonstrated that at 350 °C the catalyst is somehow oxidized. CO was produced when a pulse of CO_2 was fed on the reduced CeO_2 (the CeO_2 was pre-reduced by CO). In addition, O. Demoulin et al. [23] showed that pure CO_2 is capable to oxidize reduced (under H_2) Pd/$Ce_{0.21}Zr_{0.79}O_2$ catalyst at 300 °C. Nevertheless, the key factor is again the kinetics of the oxidation as 34 min are necessary to oxidize completely the solid (instead of 12 min under O_2). Otherwise, Staudt et al. [27] claimed that CO_2 is activated in the defect sites of ceria, even without noble metals, if the concentration of Ce^{3+} is high enough. Otsuka et al. [13] showed almost total oxidation of CeO_2 by CO_2 at 450 °C with the formation of CO (after reduction by CH_4 at 700 °C), getting a recovery degree of about 82%.

As in co-feed DRM, efforts should be focused on developing processes with transition metals instead of expensive Pt. Although Ni/CeO_2 catalysts have been thoroughly studied for reforming reactions, they have, to the best of our knowledge, never been considered for chemical looping dry reforming of methane for syngas production.

Therefore, we propose to explore the properties of Ni/CeO_2 as oxygen vector for this reaction. Before developing the experimental aspects an overview of the thermodynamics of such system is necessary. Results obtained for such Ni/CeO_2 based catalysts prepared by impregnation are then presented and discussed on the basis of different experimental parameters such as reaction temperature or Ni loading.

2. Experimental

2.1. Catalysts preparation

All the catalysts were prepared by precipitation of CeO_2 and wetness impregnation of the Ni on the homemade support. Ceria

oxide catalyst support was synthesized using triethylamine (TEA) $(C_2H_5)_3N$, (Sigma-Aldrich, ≥99.5% assay) as the precipitant agent. As an example of this synthesis, 21.9 g of cerium (III) nitrate hexahydrate $CeN_3O_9{\cdot}6H_2O$ (Fluka, >99% assay), was dissolved into 0.1 L distilled H_2O. Separately, 0.1 L of methanol CH_3OH (Sigma-Aldrich, ≥99.8% assay), as the media agent, was mixed with 0.0278 L of TEA. The solution of cerium nitrate hexahydrate was added slowly (around 1 drop/s, vigorous stirring) into the mixing of methanol and TEA. Once the addition was completed, the stirring was kept during 2 h more. The obtained solid was washed with distilled water and methanol. The product was filtered under vacuum and then dried during 24 h at 100 °C. The solid was calcined at 500 °C during 4 h in air with a heating ramp of 5 °C/min.

Nickel was loaded to ceria by the wet impregnation method. In this case, $Ni(NO_3)_2{\cdot}6H_2O$ (Sigma-Aldrich, ≥98.5%) was used as a precursor. The proper amount of $Ni(NO_3)_2{\cdot}6H_2O$ was dissolved in water, then 1 g of ceria was added to it. The mixture was stirred during 1 h. Afterwards, the water was evaporated at 60–70°. Then, the solid was removed from the beaker and dried in the oven during 1 h at 100 °C. Finally, the catalyst was treated by calcination at 500 °C during 4 h in air with the heating ramp of 5 °C/min. Three ranges of Ni loading were considered: low (2.1 wt%), intermediate (8–11 wt%) and high (38.5 wt%). In the intermediate range results shown concern three different batches with respectively 8.8, 9.5 and 10.5 wt% of Ni.

2.2. Catalysts characterization

The crystalline phases of the catalysts were measured by X-ray diffraction (XRD) using a Bruker D8 Advance X-ray diffractometer equipped with a fast detector type LynxEye with a copper anticathode. The analysis was made in the 2θ domain (20–90°) with a step of 0.02° and time integration of 0.3s. The average crystallites sizes of CeO_2, NiO and Ni^0 were estimated from the XRD patterns by Scherrer equation.

N_2 physisorption at 77 K data were collected on a multipoint and monopoint equipment to obtain the surface area of the different catalysts before and after test.

The metal loadings for all the catalysts were analyzed by X-ray fluorescence (XRF) or inductively coupled plasma (ICP) techniques.

The behavior under H_2 of these catalysts was also studied by Temperature Programmed Reduction (TPR) on a Micromeritics Autochem II Chemisorption analyzer, the H_2 consumed was analyzed by a TCD detector. 25 mg of sample was treated under a flow rate of 50 mL/min (5% H_2/N_2). The temperature was increased at a rate of 10 °C/min up to 900 °C.

The X-ray photoelectron spectroscopy (XPS) analyses were performed using a Kratos Analytical AXIS Ultra^{DLD} spectrometer. A monochromatized aluminum source (AlKα = 1486.6 eV) was used for excitation. The X-ray beam diameter is around 1 mm. The analyzer was operated in a constant pass energy of 40 eV using an analysis area of approximately 700 × 300 μm. Charge compensation was applied to compensate for the charging effect occurring during the analysis. The C 1s (285.0 eV) binding energy (BE) was used as internal reference. The spectrometer BE scale was initially calibrated against the Ag $3d_{5/2}$ (368.2 eV) level. Pressure was in the 10^{-10} Torr range during the experiments. Simulation of the experimental photopeaks was carried out using Casa XPS software. Quantification took into account a nonlinear Shirley background subtraction.

Raman spectra were recorded at room temperature with the 647.1 nm excitation line from a Spectra Physics krypton ion laser with 3 mW laser power at the sample. The beam was focused on the compounds using the macroscopic configuration. The scattered light was analyzed with an XY 800 Raman Dilor spectrometer equipped with an optical multichannel detector (liquid nitrogen-cooled charge coupled device). The spectral resolution was approximately 0.5 cm^{-1} in the investigated 200–1000 cm^{-1} range.

2.3. Catalytic chemical looping dry reforming of methane (CLDRM)

The catalytic test was conducted under atmospheric pressure in a fixed-bed quartz reactor fitted in a programmable oven. 50–200 mg of sieved solid were mixed with SiC to keep the catalytic bed volume constant. The gas stream was switched periodically between neutral gas (Ar 100%) to one containing CH_4 (5 vol%) named "reductant step" or CO_2 (5 vol%) named "oxidant step". He (5 vol%) was introduced together with CH_4 and CO_2 in order to allow internal calibration of the reactant flows. The total flow rate was maintained constant (F_T = 100 mL/min). This kind of method is one of the easiest ways of doing such process in the laboratory scale. The outlet gases were analyzed online by a mass spectrometer (QMS200 from Pfeiffer).

Typically, each cycle consisted in exposing the sample to CH_4 for 1 min, Ar for 2 min, CO_2 for 1 min and again Ar for 2 min. Cycles were repeated 12 or 60 times. The conversion of each reactant was integrated on a full cycle as well as the production of products. Ideally the conversions of CH_4 and CO_2 should be equal. The H_2/CO ratio reported is the one measured during the reductant step and should ideally be equal to 2. Other relevant values are reported for each cycle. In particular, the $C_{deposited}/C_{converted}$ ratio corresponding to the proportion of converted methane transformed in carbon during the reductant step. This value is obtained by calculating the mass balance of all carbon containing species. $CO/(CO_2 + CO)$ ratio in the reductant step is indicative of the selectivity towards partial oxidation. Ideally, it should be equal to 1 and lower values are indicative of total oxidation. Finally, $CO/CO_{2converted}$ ratio in the oxidant step is indicative of eventual carbon deposit oxidation (>1), ideally it should be equal to 1. All data are obtained with an error margin of $5\%_{rel}$.

3. Results and discussion

3.1. Thermodynamics

The first step of such study consists in determining the potential constituents of solids based on thermodynamics regarding the feasibility of the oxidation and reduction by CO_2 and CH_4 respectively.

Dry reforming of methane is an endothermic reaction which needs to be carried out at high temperature, typically above 600 °C and it can be limited by the thermodynamic equilibrium. Furthermore, as mentioned, other reactions may take place in these conditions, such as RWGS, methane cracking or the Boudouard reaction. Thermodynamics of classical co-feed DRM are well known and have been extensively reported in the literature [e.g. 2]. We will thus limit the discussion to those elements which are relevant to the understanding of the periodic behavior of the system.

The set of the standard Gibbs free energy was calculated using the "*factsage.com*" [28] website database. $\Delta_f G°$ at 600 °C, 700 °C and 800 °C for several relevant reactions are reported in Table S1.

DRM (reaction ***(1)*** in Table S1) becomes favorable around 650 °C. Cracking of methane is more favorable than DRM up to 725 °C, which is one of the reasons about obtaining less carbon at high temperatures. In addition, the oxidation of the deposited carbon with CO_2 ***(2)*** is favorable above 700 °C but more difficult to occur thermodynamically than carbon deposition ***(3)*** in the whole working range. Therefore, the eventual carbon would be quite difficult to oxidize at the same time as the DRM occurs due to the competition

between CH_4 and C to react with CO_2, as the one of CH_4 is more favorable.

Moreover, the absolute $\Delta_f G^\circ$ of RGWS ***(4)*** is very small in all the temperature range. Thus, 100% selectivity towards syngas is quite difficult to reach from the thermodynamic point of view in the classical DRM process.

The chemical looping dry reforming of methane (CLDRM) system needs particular properties. The solid plays a role as a reactant of the reaction (besides the catalytic properties of activating CH_4 and CO_2, in this case separately). The following calculations are based on known solid phases for which thermodynamic data is available. For ceria, two redox systems (CeO_2–Ce_6O_{11} and CeO_2–Ce_2O_3) are considered.

3.1.1. Reactivity of Ni species

Table S1 shows that the total oxidation of methane towards H_2O and CO_2 ***(7)*** is the most favorable to occur within the different possible pathways to reduce NiO ***(5, 6 and 7)***. Unless the selectivity is somehow controlled by kinetic means, this shows that, at first sight, Ni-NiO system is not adapted to act as an oxygen vector for CLDRM.

On the other side, Table S1 shows that the oxidation of Ni^0 to NiO by CO_2 ***(8)*** is not favorable in the temperature range explored. This is a crucial property from the selectivity point of view. Indeed, the unselective reduction of NiO towards Ni producing H_2O and CO_2 would occur only once, at the beginning of the experiment. On this way, Y.H. Taufiq-Yap et al. [29] observed Ni^0 without any peak of NiO in the XRD patterns after DRM experiment. Obviously, the re-oxidation of Ni° by O_2 ***(9)*** is feasible in the whole range of temperature considered. This type of behavior can be also correlated with the literature. Bhavsar et al. [16] studied the chemical looping combustion (thus re-oxidizing the catalyst with air) over Ni-CeO_2. They showed clearly the production of CO_2 which is in concordance with the reduction of NiO to produce water and carbon dioxide. Regarding Ni, it can therefore be deduced that except during a first reduction step to Ni°, nickel will not act as an oxygen vector for CLDRM. It may nevertheless play an important role on the reactivity point of view.

3.1.2. Reactivity of Ce species

The partial oxidation of CH_4 on CeO_2 to Ce_2O_3 ***(10)*** is more favorable than the total oxidation ***(11 and 12)***. Moreover, the selective oxidation of methane between CeO_2 and Ce_6O_{11} ***(13)*** is even more favorable than the direct reduction of CeO_2 to Ce_2O_3 ***(10)***. In this context, Otsuka et al. [13] showed that the oxidation of CH_4 over CeO_2 becomes feasible at temperatures above 650 °C, which is quite close to our calculations (680 °C for reaction ***(13)***). In all cases the selective oxidation of methane towards syngas is more favorable than total oxidation, making CeO_2 a good candidate to act as oxygen vector in CLDRM.

Obviously, the other main reaction is the re-oxidation of Ce_xO_y by CO_2 ***(14, 15, 16)***, which in all the cases is thermodynamically favorable at the working temperature range (600–800 °C). Moreover, the Ce_xO_y oxidation is more feasible at lower temperature. Nevertheless, the variation of the Gibbs free energy on the oxidation of Ce_6O_{11} to CeO_2 is really close to zero, meaning that some thermodynamics limitations can be expected in this case. As a reference, Otsuka et al. [13] demonstrated that the reduced ceria on a Pt-CeO_2 catalyst can be oxidized by CO_2. Otherwise, NiO and Ce_xO_y ***(17, 18)*** are always in favor of Ni species reduction, which should maintain Ni in metallic state if no O_2 is present. Furthermore, it can be seen that ceria will not oxidize carbon eventually deposited at its surface ***(9, 20)***.

In summary, Ni-CeO_2 system appears to be a very good candidate for Chemical Looping DRM although it is known to be a good catalytic solid towards CLC. The main difference is that in the case of the re-oxidation by CO_2, NiO cannot be formed and CeO_2 acts as an unique potential oxygen vector which is selective to syngas production.

It must be underlined that such thermodynamic considerations are based on known and stable phases for which thermodynamic data is available. One cannot exclude the existence, in the working conditions, of other phases with reactivities in favor or disfavor of CLDRM.

3.2. Catalysts characterization

The Table 1 summarizes the main properties of the Ni/CeO_2 catalysts.

The X-ray diffraction patterns of the different Ni loaded compounds (Fig. 2) evidence characteristic fluorite structure of CeO_2 in all the cases. NiO is not observed at the lowest nickel content which could be explained by several reasons: (i) the particles may be too well dispersed on CeO_2 to be detected, (ii) a solid solution of cerium and nickel could be formed, or (iii) the particles may be amorphous. At higher loadings, narrow peaks of NiO are observed at 36.8°, 43.2°, 63.1° and 75.4° with average crystallites sizes of 21, 16 and 18 nm for Ni(38.5)/CeO_2, Ni(8.8)/CeO_2 and Ni(9.5)/CeO_2, respectively. The same average crystallites size for CeO_2 (12 nm) is obtained at high (38.5%) and low (2.1%) loadings of nickel. In addition the surface areas of the catalysts are similar, 27 m^2/g for Ni(2.1)/CeO_2 and 33 m^2/g for Ni(38.5)/CeO_2 to the ones observed for Ni(8.8)/CeO_2 (29 m^2/g) and Ni(9.5)/CeO_2 (32 m^2/g). Thereby, the loading of nickel, at least even up to 38.5%, does not seem to affect the total surface area of the catalyst using the impregnation method. Furthermore, the reproducibility of this method is checked comparing the properties of the Ni(8.8)/CeO_2 and Ni(9.5)/CeO_2, which shows almost identical XRD patterns, average crystallites sizes and surface areas. However, compared to ceria alone adding Ni leads to an increase of the average crystallites size and a decrease of the specific surface area.

The TPR of Ni(38.5)/CeO_2, Ni(9.5)/CeO_2 and Ni(2.1)/CeO_2 (Fig. 3) show two peaks between 265 and 365 °C which are related to the reduction of nickel species. While the peak related to reduction of ceria is at 794 and 800 °C for 38.5 wt% Ni and 2.1 wt% Ni, respectively. It is significantly lower for 9.5 wt% Ni (766 °C). Large NiO crystallites seem to be more difficult to reduce as the main peak related to the reduction of nickel shifts from 315 °C for Ni(2.1)/CeO_2, assuming nickel is present as NiO at such low content, going to 327 °C for Ni(9.5)/CeO_2 and 362 °C for Ni(38.5)/CeO_2. The lowest is the Ni loading the lowest is the temperature of reduction (362 °C → 38.5 wt% Ni, 327 °C → 9.5 wt% Ni and 315 °C → 2.1 wt% Ni). Otherwise, the peak found around 270 °C could be attributed to the presence of Ni species in very small NiO crystallites and/or in a Ce-Ni-O solid solution [30,31]. Therefore, it appears that in all the studied compounds, there are some Ni species in strong interaction with Ce species that can be found at the interface between NiO and CeO_2 or in Ce-Ni-O solid solution.

3.3. Catalytic performances in CLDRM

3.3.1. Activity of CeO_2

The role of the CeO_2 without an active metal was investigated. The experiments were carried at 700 °C, 750 °C and 800 °C. Fig. S1 shows the partial pressures in the outlet of the reactor at 800 °C. The other two experiments are not shown as the activities were negligible.

Comparing the reaction cycles to the first one performed with the closed reactor (by-pass), it can be seen that the partial pressures of CH_4 and CO_2 rapidly reach the nominal value in each reductant and oxidant step. Indeed, the conversions of CH_4 and CO_2 are around 0.5–1%.

Table 1
Ni loading, surface area (BET) and average crystallites size (from XRD) of the different catalysts

Catalyst	Ni loading (wt.%)	Ni/M_T Atomic ratio	S_{BET} (m^2/g)	d_{NiO} (nm)	d_{CeO2} (nm)
CeO_2	–	–	53	–	6
Ni(2.1)/CeO_2	2.1	0.06	27	n.o.	12
Ni (8.8)/CeO_2	8.8	0.22	29	16	11
Ni(9.5)/CeO_2	9.5	0.24	32	18	10
Ni (10.5)/CeO_2	10.5	0.26	35	n.a.	n.a.
Ni(38.5)/CeO_2	38.5	0.65	33	21	12

n.o.: not observed. n.a.: not analysed.

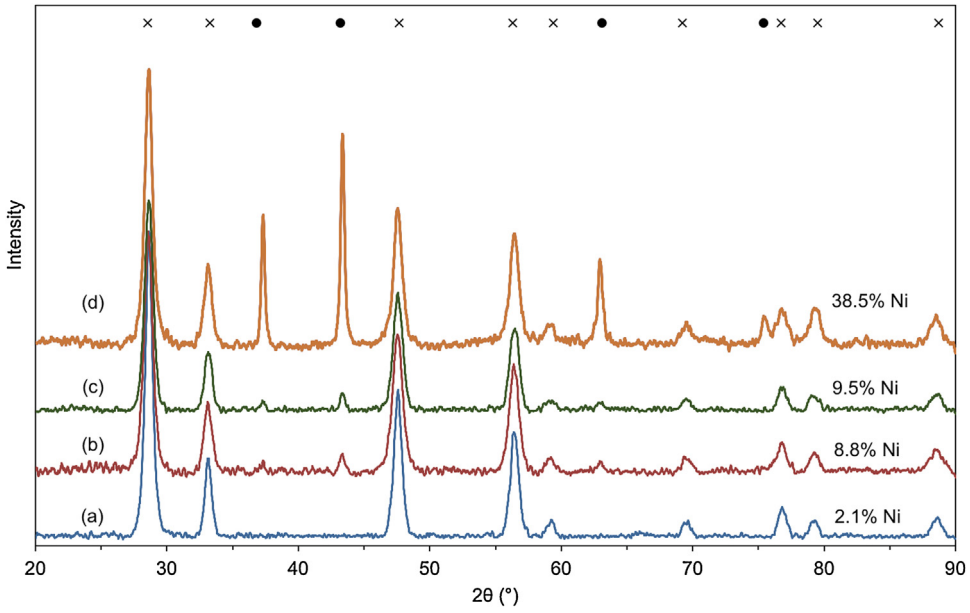

Fig. 2. XRD patterns for (a) Ni(2.1)/CeO_2, (b) Ni(8.8)/CeO_2, (c) Ni(9.5)/CeO_2, (d) Ni(38.5)/CeO_2 x CeO_2 ● NiO.

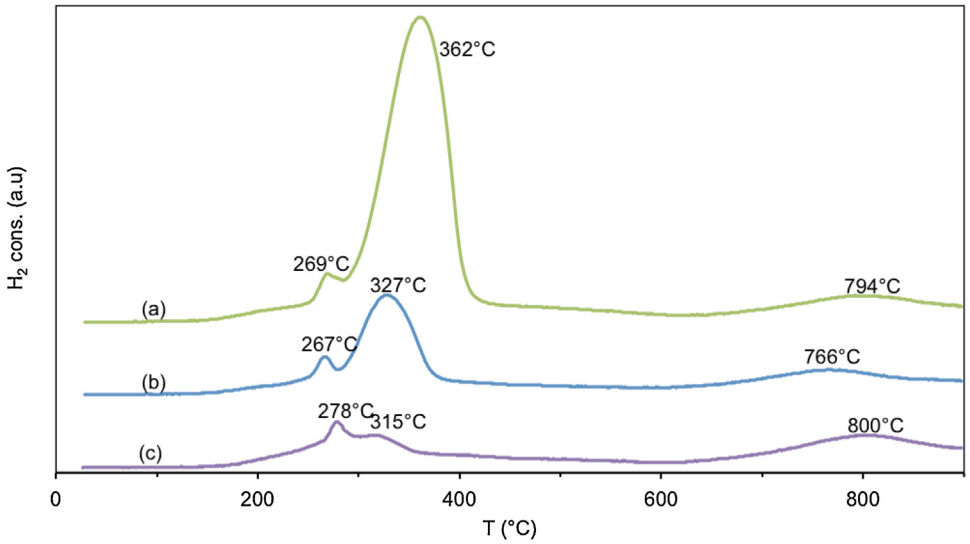

Fig. 3. TPR profile of (a) Ni(38.5)/CeO_2, (b) Ni(9.5)/CeO_2, (c) Ni(2.1)/CeO_2 under 10% H_2/N_2 gas.

3.3.2. *Activity of Ni/CeO_2*

The partial pressures of the different compounds along the whole experiment are represented in Fig. 4 for Ni(8.8)/CeO_2 at 700 °C. The reactive cycles are preceded and followed by cycles with the reactor closed in order to calibrate the MS signals.

The experiment starts showing a different behavior for the first redox cycle in respect to the following ones. A considerable amount of H_2O and CO_2 is produced during the first reductant step (CH_4) but decreases down to almost zero after the first 2 cycles, leading to a highly selective system towards syngas products. It should be reminded that the catalysts used were not pre-reduced before test. Therefore, the production of H_2O and CO_2 in this first cycle can be ascribed to the reduction of NiO species that are subsequently not re-oxidized by CO_2 as could be expected by the thermodynamics

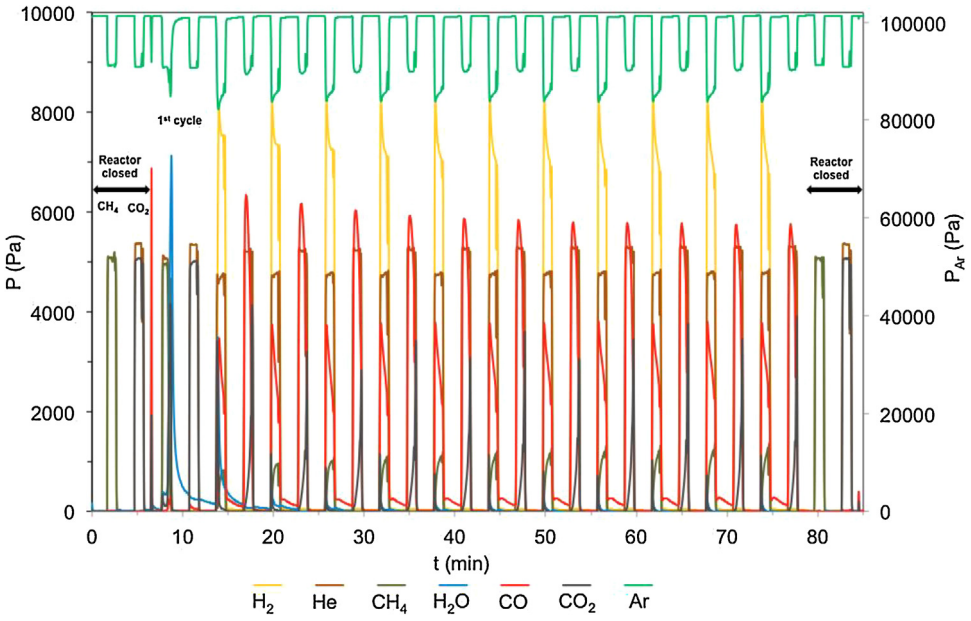

Fig. 4. Partial pressures in the outlet flow working with 200 mg of Ni(8.8)/CeO_2 (0.1–0.2 mm) + 100 mg SiC at 700 °C $F_{T,0}$ = 100 mL/min. Cycle: 1 min 5% CH_4, and 1 min 5% CO_2.

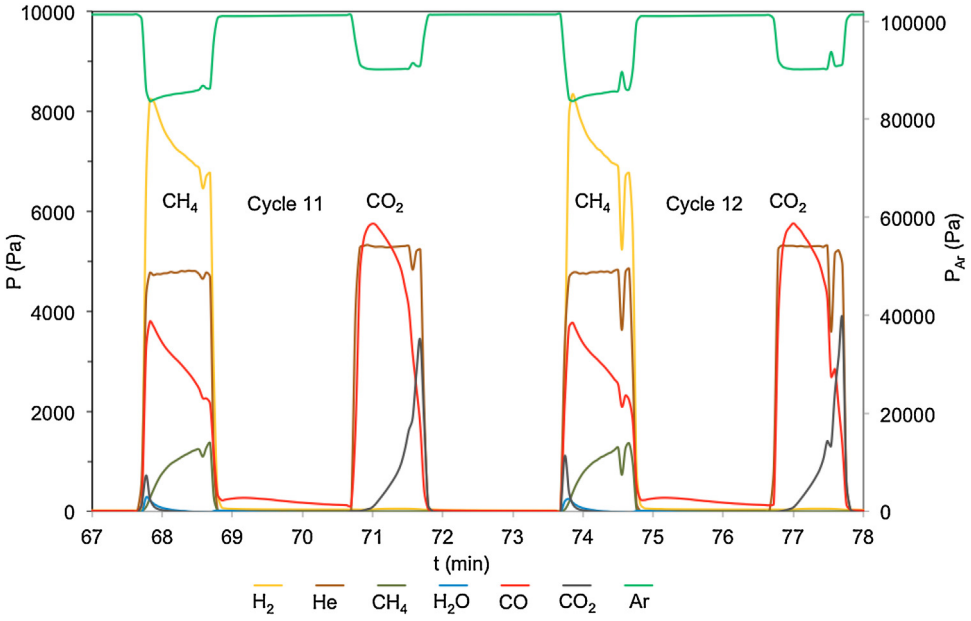

Fig. 5. Partial pressures in the outlet flow, zoom of Fig. 4.

calculations. V. Galvita et al. [32] also observed H_2O and CO_2 in the early stage of the reaction working with Pt-Ce-Zr based catalyst on the periodic SRM. The absence of total oxidation products in the successive cycles is consistent with the hypothesis that in such reaction condition Ni° species are not oxidized to NiO. These results also confirm that CeO_2 may play the role of selective oxygen vector for syngas production by CLDRM as the system tends to become almost 100% selective towards H_2 and CO during the reductant steps with an almost negligible production of H_2O and CO_2. Fig. 5 shows a zoom in the last two cycles of the experiment in order to verify the excellent reproducibility from one cycle to the other.

First, H_2 and CO are produced majorly during the reductant step with a really small contribution of H_2O and CO_2. The same production of H_2 and CO is obtained for the two cycles showing a remarkable reproducibility between the two, even after 10 cycles. In addition, the production of CO decreases progressively during the reductant step which can be due to a lack of oxygen in the carrier. However, in this experiment the amount of oxygen in CeO_2 (2064 μmols) is largely enough to react with the CH_4 feed (205 μmols). Even considering the redox couple between CeO_2 and Ce_2O_3 where only 25% of the oxygen in CeO_2 is released, the oxygen available is still high (516 μmols O) which is not the case if the reduction to Ce_6O_{11} is considered (172 μmols O).

On the other side, the CO_2 partial pressure does not reach the nominal value of 5000 Pa during the oxidant step. Probably, CO_2 needs more time to oxidize completely the Ce_xO_y species at the given working conditions. As expected, there is an important production of CO during this step due to the oxidation of Ce_xO_y species

and, eventually, of some carbon deposited during the reductant step.

A graph with the main values of conversion and selectivity is shown in Fig. 6. In practice, the properties from the reductant step in the cycle 1 are shown above the number 1 along the x-axis, whereas the properties for the oxidant step in the cycle 1 are shown above the number 1.5 along the x-axis to differentiate between the two and to not get confused with classic results of DRM in co-feed.

There is an evolution of the conversion between the first cycle and the following ones. During the first cycle 28% conversion of CH_4 and only 9% of CO_2 are obtained, so relatively low conversions are obtained on the oxidized compound. Then, the two become stable around 80% until the end of the experiment, showing an activation phenomenon with increasing conversions. Besides, H_2/CO ratio goes from 3.2 in the first cycle to 2.2 in the last one. Even though H_2/CO is equal 3.2, the ratio CO/(CO_2 + CO) is almost zero, meaning that there is no or negligible production of CO. Therefore, the H_2/CO value at that first cycle is not relevant as it would come from some residual production of CO. Otherwise, the selectivity between H_2, CO, H_2O and carbon deposit become more coherent from the cycle 2. Indeed, the CO/(CO_2+CO) ratio goes close to 1 (0.98), which corroborates the small production of CO_2. The $C_{deposited}/C_{conv.}$ (%) decreases from 15% in the cycle 2 to 8% in cycle 12, at the same time the H_2/CO ratio decreases from 2.5 to 2.2. This trend is coherent considering that if less cracking of methane occurs in the system, less production of hydrogen would come from this reaction. In addition, the low deposition of carbon during the reductant step is also corroborated thanks to the $CO/CO_{2,conv}$ ratio obtained in the oxidant step, which goes around 1.1. Such value means that almost all the CO_2 oxidizes the ceria species and only a small amount is used to oxidize the carbon deposit.

Moreover, Fig. S2 shows the instantaneous conversions in order to follow the behavior of the reactants within the step.

The conversion of CH_4 goes from 100% to around 70% evidencing the dynamic behavior of the periodic process. Probably, the kinetic is faster when ceria is totally oxidized and then it is slower as the oxygen reservoir starts to decrease. In addition, obtaining 100% conversion at the beginning of the reductant step in each cycle reinforces the advantage of working in a dynamic process from the thermodynamic point of view, as the limitations are more difficult to reach than working in co-feed (stationary state). From the other side, the CO_2 conversion goes almost to zero at the end of the oxidant step. This trend is favorable for our interest. CO_2 conversion going to zero would mean that all the species are re-oxidized and the use of CO_2 is close to optimal. Therefore, this experiment is a good opportunity to compare the mass balance on the catalyst towards oxygen and carbon in the whole cycle.

The Fig. S2 also shows that the overall approx. 80% conversions of CO_2 and CH_4 (Fig. 6) are not due to thermodynamic limitations as would occur in classical DRM. Indeed, if the steps had been shorter, the integrated conversion would have given higher values, eventually reaching 100%. This is an important point to take into account in comparing classical DRM performances to CLDRM.

Table 2 shows the mass balance of oxygen and carbon in the catalyst during the two steps of the last four cycles. The amount of oxygen released in the reductant step is near to that inserted during the oxidant step. In addition, the amounts of carbon deposited during the reductant step correspond to those oxidized during exposure to CO_2 this indicates that carbon does not accumulate on the surface of the solid in these experimental conditions. Mass balances thus confirm the hypothesis about CO_2 being capable to oxidize both the reduced ceria and the eventual carbon deposit in such conditions. In an overall view, this experiment has shown the principles and the procedures that we follow to process and understand the data of the different experiments in periodic. Besides, the experiment shown demonstrates the feasibility of working in such conditions even at 700 °C, obtaining promising conversions and selectivity.

Supporting Ni species on CeO_2 allows drastically increasing CH_4 and CO_2 conversions as conversions of about 1% were obtained on CeO_2 alone (Fig. S1). Clearly, Ni species have an essential role in the activation of the reactants. Besides, CeO_2 playing the role of selective oxygen vector for syngas production furnishes the O species which leads to the creation of anionic vacancies in the solid. Activation of CH_4 on Ni species is expected, however CO_2 activation that has been proposed on anionic vacancies [33–35] is also largely enhanced in the presence of Ni species. This could be explained by the presence of Ni species in strong interaction with Ce species increasing the number of anionic vacancies in CeO_2 and/or in the Ce-Ni-O solid solution.

3.3.3. Stability test

A 60 cycles experiment instead of 12 were carried at 800 °C on Ni(8.8)/CeO_2 in order to check the stability of the process (Fig. 7). The conversions of CH_4 and CO_2 reach 95% and 99%, respectively. In addition, around 100% selectivity is found obtaining H_2/CO = 2.0, CO/(CO_2 + CO) = 0.96 and $C_{deposited}/C_{conv.}$ = 4%. The performance underlines clearly the feasibility of DRM in periodic conditions with the advantages associated, such as avoiding the RWGS. Interestingly the proportion of coke formed diminishes along the cycles.

3.3.4. Characterization of catalysts after reduction and oxidation steps

In order to characterize the state of the catalyst and eventual differences after the reduction and oxidation steps, a series of four separate experiments were performed using 200 mg of Ni(10.5)/CeO_2. CLDRM was performed at two different temperatures (600 °C and 800 °C) and stopped at the convenient moment (i.e. after a reduction or oxidation step) after 30 cycles in order to be sure that the solid is "stable" in terms of the internal evolution. Samples were cooled down to room temperature in flowing argon.

3.3.4.1. XPS. Cerium compounds have XPS spectra with rather complex features due to numerous initial and 4f electronic configurations. The 3d spectrum, registered on pure ceria, can be resolved into three spin-orbit doublets, $3d_{3/2}$-$3d_{5/2}$, noted (u, v), (u", v") and (u"', v"'). Fig. S3 shows the Ce $3d_{3/2.5/2}$ spectrum, observing the typical pattern of Ce^{4+} species before experiment. The characteristic peak of Ce^{4+} is observed at 916.7 eV. Typically, this peak does not appear for the Ce^{3+} spectrum [36,37]. Such peak appears in all the cases after experiment. On the other hand, typical peaks for Ce^{3+} (u°, v°, u' and v' at 899.1, 880.9, 903.4 and 885.2 eV, respectively) are absent from all the XPS spectra. Therefore, the surface CeO_2 is apparently not reduced to Ce^{3+}. This could be explained by a rapid diffusion of oxygen species from the bulk towards the surface of the solids during the cooling of the reactor. Indeed, surface Ce_xO_y can be slowly oxidized even feeding only noble gases, just because of the oxygen diffusion from the bulk [22]. A long reduction by methane or/and an in-situ XPS experiment seem to be necessary to reach Ce^{3+} species on the first layers of the catalyst.

Fig. 8 gathers the XPS spectra for Ni 2p, O 1s and C 1s for all the samples, whereas the corresponding quantitative data is presented in Table 3.

Compared to the initial state, a decrease in Ni concentration (Table 3) is seen on all samples after reaction which can be attributed to particles sintering. Indeed, the surface area of the samples decreases drastically from approx. 32 m^2/g to approx. 2 m^2/g after test. Partial coverage of Ni species by carbon could also explain such lowering. C is observed on all samples including the calcined catalysts. Part of this C can thus be due to contamination in handling or in the analytical instrument, and it is usually used as an inter-

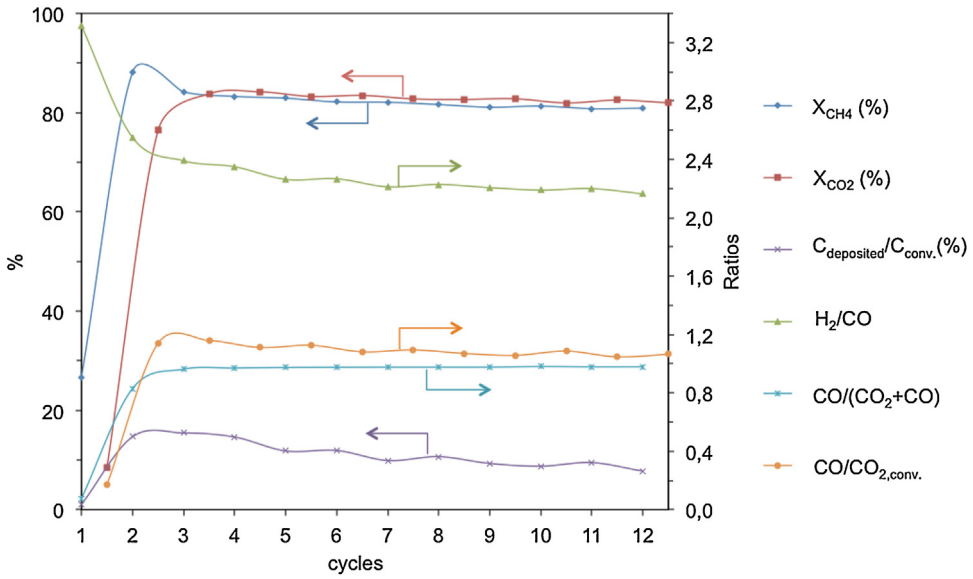

Fig. 6. Reductant step: Conversion of CH_4 (%), $C_{deposited}/C_{conv.}$(%), H_2/CO and $CO/(CO_2+CO)$ ratios. Oxidant step: Conversion of CO_2 (%) and $CO/CO_{2,conv}$. ratio. 200 mg of Ni(8.8)/CeO_2 (0.1–0.2 mm) + 100 mg SiC at 700 °C $F_{T,0}$ = 100 mL/min. Cycle: 1 min 5% CH_4, and 1 min 5% CO_2.

Table 2
Catalyst mass balance of oxygen and carbon for the last four cycles of the experiment.

Cycle n.	Oxygen mass balance (±5% μmols)			Carbon mass balance (±5% μmols)		
	Reductant	Oxidant	Full cycle	Reductant	Oxidant	Full cycle
9	−152	165	13	15	−13	2
10	−153	152	−1	14	−17	−3
11	−151	166	15	15	−11	5
12	−154	158	3	13	−13	0

Mass balances: positive = uptake by solid, negative = supply by solid.

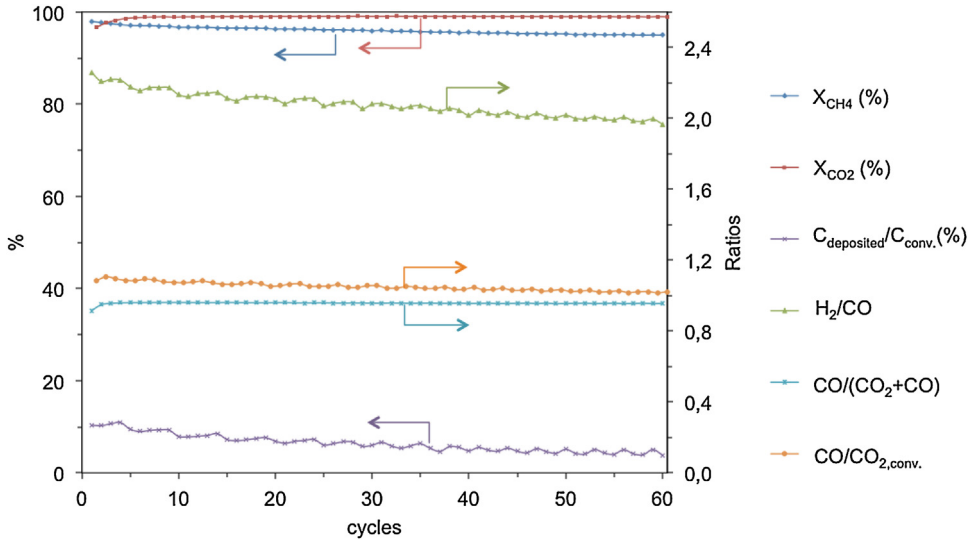

Fig. 7. Reductant step: Conversion of CH_4 (%), $C_{deposited}/C_{conv.}$(%), H_2/CO and $CO/(CO_2+CO)$ ratios. Oxidant step: Conversion of CO_2 (%) and $CO/CO_{2,conv}$. ratio. 200 mg of Ni(8.8)/CeO_2 (0.1–0.2 mm) + 100 mg SiC at 800 °C $F_{T,0}$ = 100 mL/min. Cycle: 1 min 5% CH_4, and 1 min 5% CO_2.

nal reference. Nevertheless, surface carbon concentration increases after reaction, in particular at 600 °C. Logically, the carbon concentration decreases after the CO_2 step. One can expect carbon to be formed preferentially in proximity of Ni species affecting the XPS response of Ni. Furthermore, graphitic carbon can be identified at 600 °C. The relative amount of such graphite type carbon is higher after CO_2 exposure indicating that such species are more difficult to remove at this temperature.

Ni $2p_{3/2}$ XPS spectra show three main contributions. The peak at 852.7 eV observed on catalysts after test can be attributed to Ni^0 species. Two Ni^{2+} species can be seen. The peak at 853.7 eV (with a multiplet split at 855.4 eV) can be attributed to Ni^{2+} from NiO. The contribution peak at 855.7 eV is usually attributed to Ni^{2+}

species from $Ni(OH)_2$ hydroxides [37,38]. This is coherent with the presence of a significant contribution of O 1s at 531.5 eV observed on all samples. However, on Ni-CeO_2 systems, such peak at 855.4 eV has also been attributed to Ni^{2+} species in strong interaction with Ce species [39–41].

The evolution of Ni species according to the last exposure (CH_4 or CO_2) can be observed at both reaction temperatures. At 800 °C the most striking evolution is the decrease after CH_4 exposure, in comparison to CO_2 exposure, of the Ni^{2+} from NiO contribution. Simultaneously, reduced Ni^0 species increase but also the Ni^{2+} with higher binding energy at 855.7 eV which would favor the hypothesis of surface hydroxides formation and/or increase of Ni^{2+} species in strong interaction. The same trend can be observed at 600 °C.

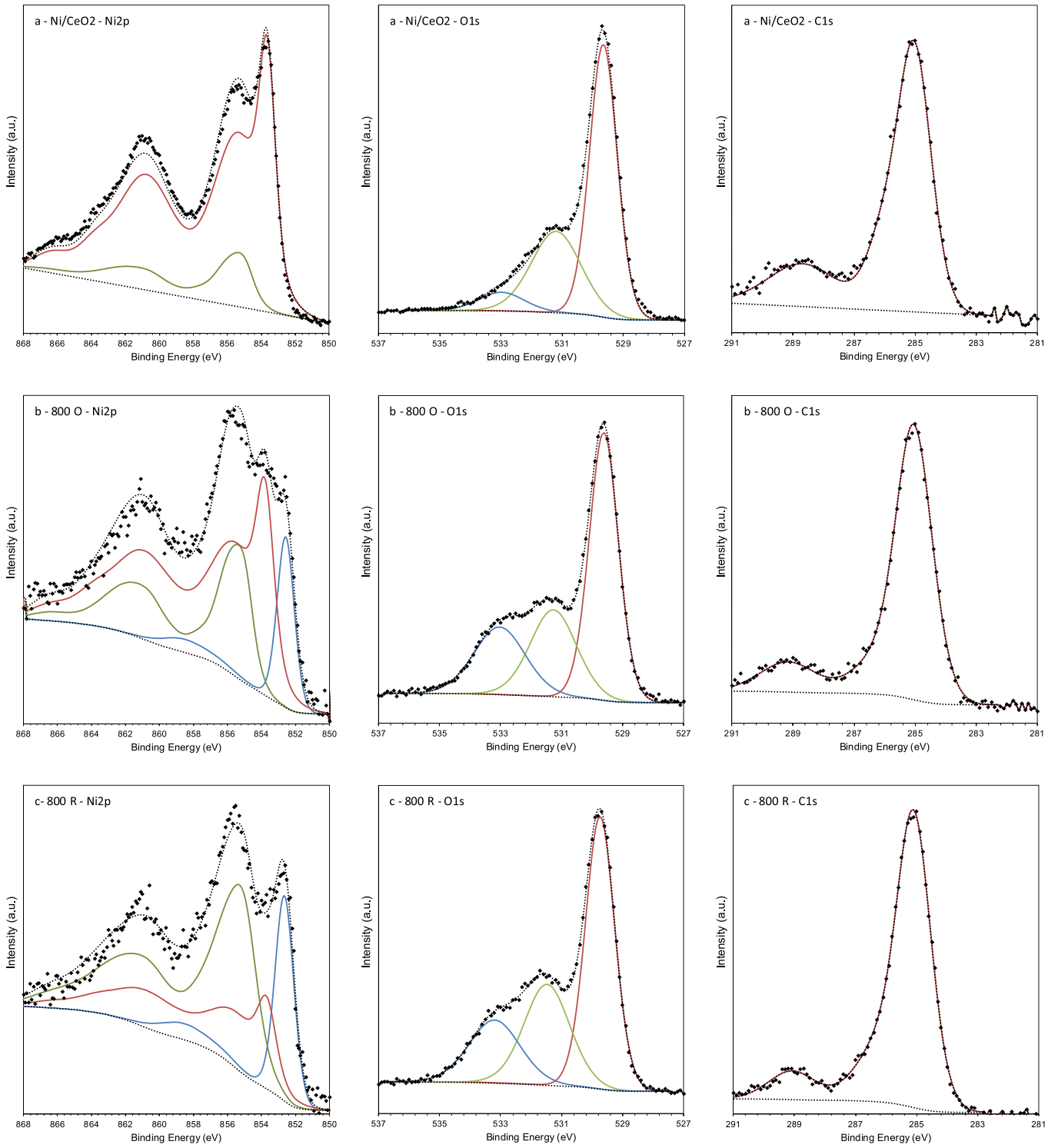

Fig. 8. XPS spectra of Ni $2p_{3/2}$, O 1s and C 1s: (a) Ni(10.5)/CeO_2 before test, (b) after CO_2 step at 800 °C, (c) after CH_4 step at 800 °C, (d) after CO_2 step at 600 °C, (e) after CH_4 step at 600 °C.

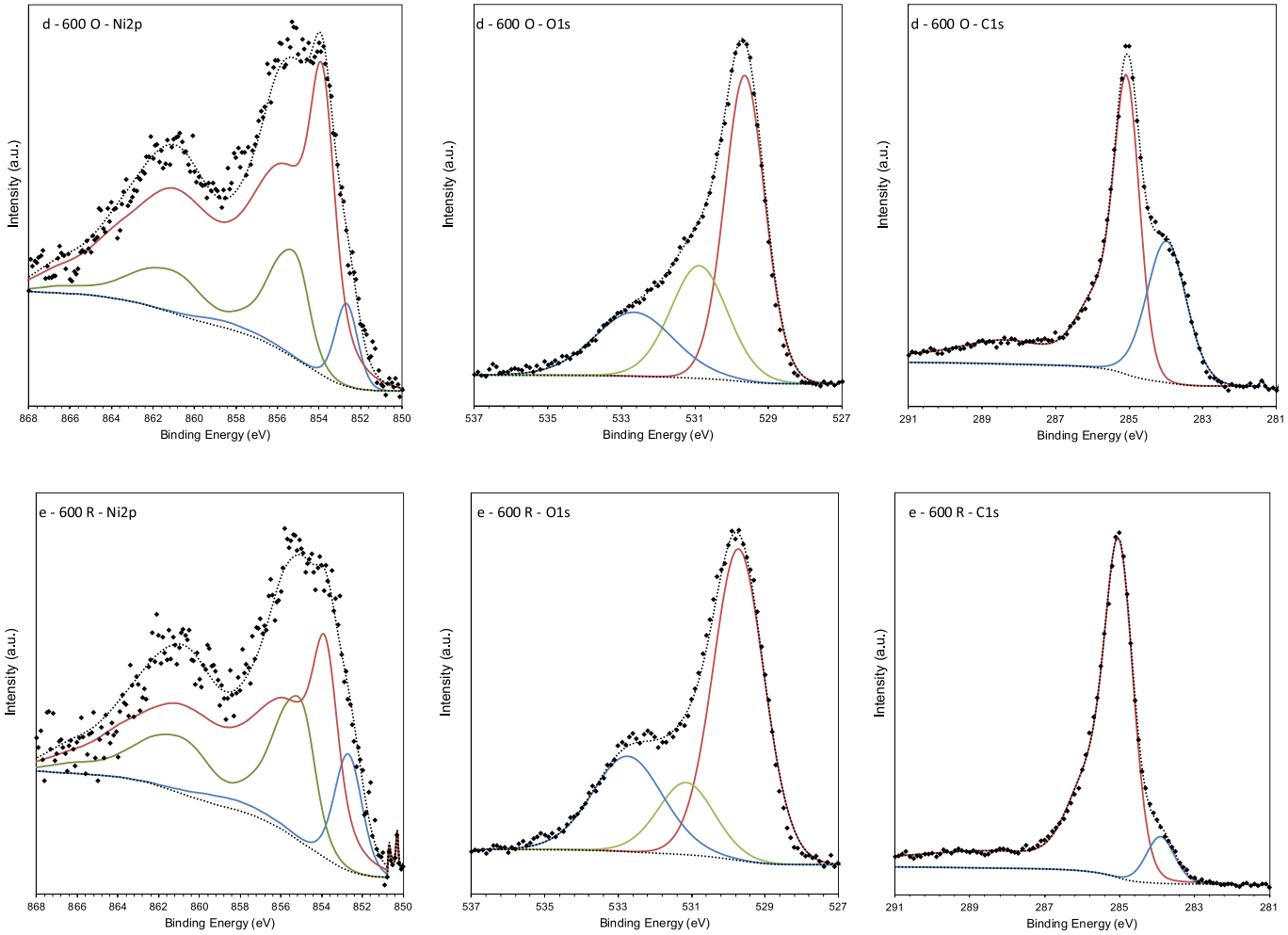

Fig. 8. (*Continued*)

Table 3
Data from XPS analysis for Ni(10.5)/CeO_2 before and after experiments.

	Surface concentrations (at%)				Atomic ratios			
Catalyst	Ce	Ni	O	C	Ni/Ce	O/Ce	C/Ce	C/Ni
Ni(10.5)/CeO_2	12	24	40	23	2.1	3.4	2.0	1.0
800 °C, after CO_2	11	11	42	36	1.0	3.9	3.4	3.3
800 °C, after CH_4	9	9	36	45	1.0	4.0	4.9	4.9
600 °C, after CO_2	11	6	31	51	0.5	2.7	4.5	8.1
600 °C, after CH_4	7	3	25	64	0.4	3.4	8.6	20.0

	Oxygen (at%)			Nickel (at%)			Carbon (at%)	
	O^{2-} 529.7 eV	OH 531.5 eV	O' 533.2 eV	Ni^0 852.7 eV	$Ni^{2+}{}_{NiO}$ 853.7 eV	$Ni^{2+}{}_{Ni(OH)2}$ 855.7 eV	C_{graph} 283.9 eV	C 285.0 eV
Ni(10.5)/CeO_2	55	40	6	0	64	36	-	100
800 °C, after CO_2	51	26	23	13	59	28	-	100
800 °C, after CH_4	50	29	20	19	28	53	-	100
600 °C, after CO_2	52	27	21	6	75	19	31	69
600 °C, after CH_4	60	15	25	11	59	30	8	92

These results also confirm [42] that surface oxidation of reduced Ni species by CO_2 is possible although bulk oxidation is not thermodynamically favorable in these reaction conditions.

3.3.4.2. XRD. Figs. 9A and B shows the XRD patterns for the different samples and that of a similar starting catalyst Ni(9.5)/CeO_2. For ceria, only the fluorite CeO_2 structure is visible. Whereas the original catalysts show the diffraction patterns for NiO, the used samples show only Ni° confirming that in the reaction condition bulk NiO is reduced and is not re-oxidized by CO_2. Fig. 9B shows in more detail the (220) diffraction peak of ceria. It can be seen that the sample reacted at 600 °C shows a slight increase of the average crystallites size (from 10 nm to 13–14 nm) and a shift towards smaller diffraction angles which are independent of the nature of

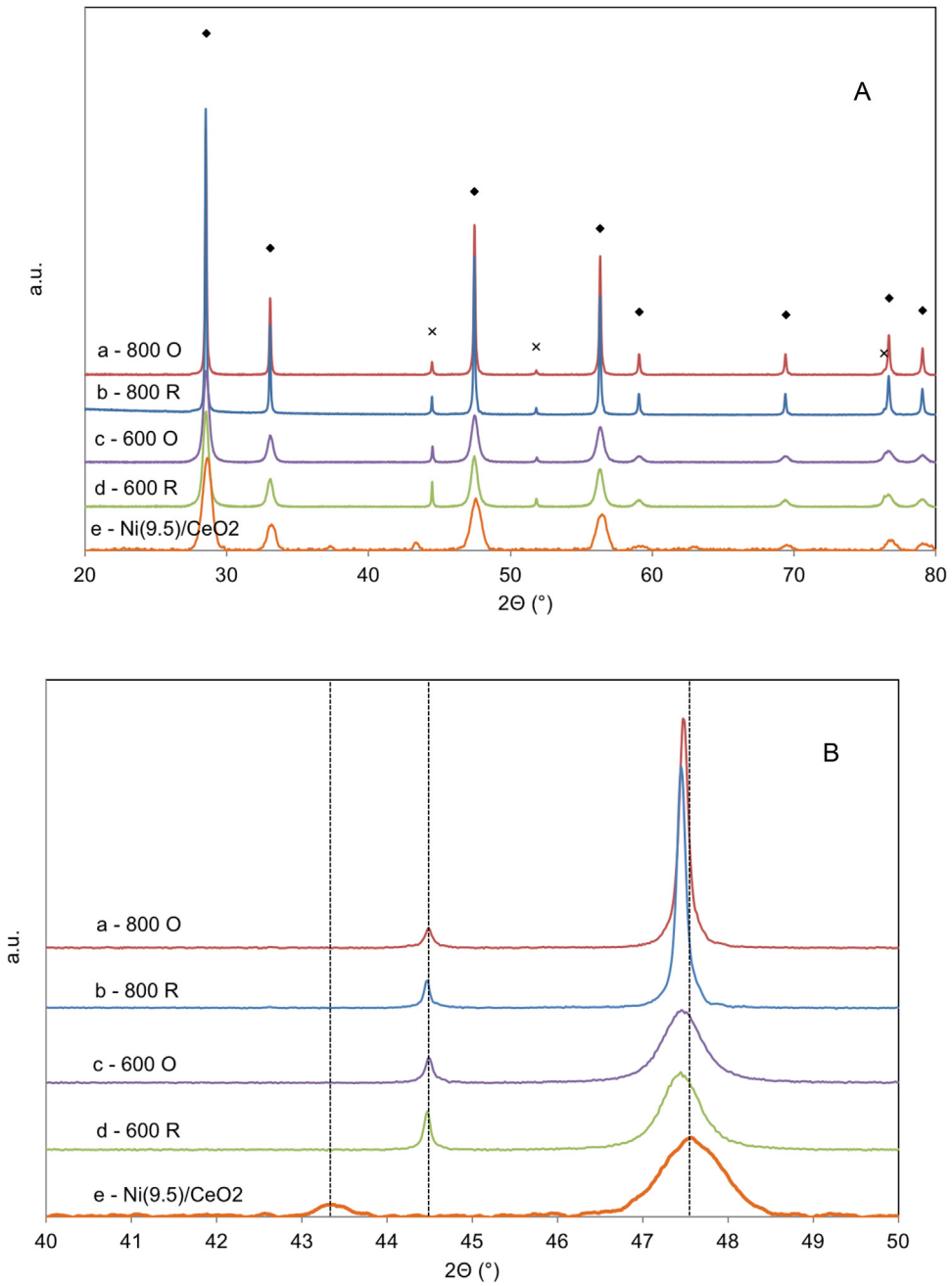

Fig. 9. XRD patterns (a) after CO_2 step at 800 °C, (b) after CH_4 step at 800 °C, (c) after CO_2 step at 600 °C, (d) after CH_4 step at 600 °C on Ni(10.5)/CeO_2 and (e) Ni(9.5)/CeO_2 after calcination – A: 2Θ = 20° to 80° B: 2Θ 40° to 50° (● CeO_2, x Ni).

the last reaction step (CH_4 or CO_2). After reaction at 800 °C, the samples logically show narrower diffraction peaks due to the sintering of the support (average crystallites sizes between 56 and 61 nm). Again, a slight shift to smaller diffraction angles is observed and is more significant after exposure to CH_4. Such shifts towards smaller angles can be attributed to the expansion of the ceria lattice [43] as a consequence of the reduction of Ce^{4+} (radius 0.97 Å) to Ce^{3+} (radius 1.14 Å). No other phases of the Ce-O system can be detected.

3.3.4.3. RAMAN scattering. Fig. 10 reports the Raman spectra recorded for the 4 samples after test as well as a calcined catalyst precursor (Ni(9.5)/CeO_2), the synthetized ceria support previous to Ni impregnation (CeO_2) and a commercial ceria.

All samples show an important band at 465 cm^{-1} band which is attributed to the symmetrical stretching mode (ν_s(Ce-O)) of the CeO_8 vibrational unit, environment of the cerium by the oxygen in the cubic fluorite lattice of ceria. Contrary to Fang et al. [31], no significant shift of this band can be observed between the samples which does not allow concluding on the eventual presence of a Ni-Ce-O solid solution as for very low Ni loading no shift was observed.

The two supports without Ni shows similar Raman spectra, with the exception that the 465 cm^{-1} band is narrower for the commercial sample due to a better crystallization with respect to the prepared support. The grain size of this latter support can be estimated to 30 nm considering relation between half-width intensity and grain size established by Kosacki et al. [44]. However, the shoulder and asymmetry towards lower wavenumbers can suggest the presence of particles below 10 nm, thus in better accordance with XRD crystallites size [45–47]. A small contribution at 596 cm^{-1} can also be detected (Table 4). This weak band is generally attributed to

Table 4
Raman analysis for CeO_2, Ni(9.5)/CeO_2 before experiments and Ni(10.5)/CeO_2 after CLDRM experiments. Particles sizes are calculated according to ref. [38]

Catalyst	ν_s(Ce–O) (cm^{-1})	D_e (cm^{-1})	D_i (cm^{-1})	Size (nm)	Surface ratios	
					A_{De}/A_{F2g}	A_{Di}/A_{F2g}
CeO_2	465.5		596.0	30		0.02
Ni(9.5)/CeO_2, before DRM	465.7	547.5	615.8	24	0.20	0.12
800 °C, after CO_2	464.9	547.4	615.8	76	0.14	0.08
800 °C, after CH_4	466.0	547.1	615.2	59	0.62	0.17
600 °C, after CO_2	465.1	542.9	600.5	27	0.48	0.37
600 °C, after CH_4	464.8	542.9	600.5	24	0.56	0.36

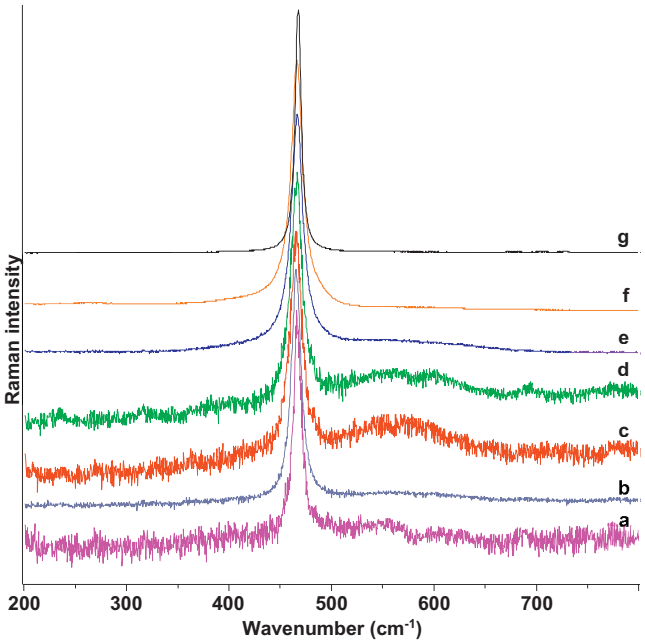

Fig. 10. Raman spectra (a) after CH_4 step at 800 °C, (b) after CO_2 step at 800 °C, (c) after CO_2 step at 600 °C, (d) after CH_4 step at 600 °C on Ni(10.5)/CeO_2, (e) Ni(9.5)/CeO_2 after calcination, (f) synthetized CeO_2 and (g) commercial CeO_2.

O^{2-} vacancy positions [46,48] or to defects in nanosized particles. This is also referred as intrinsic defect mode [49,50].

The impregnation of Ni does not affect the position of the 465 cm^{-1} band. The band is slightly narrower and more symmetrical suggesting a better crystallization. No NiO signal at approximately 520 cm^{-1} could be detected because of a shadowing effect by the long tail of the first-order CeO_2 peak. The spectra are normalized to the height of this band. However, a significant band can be observed in the 500–630 cm^{-1} region, which can be decomposed in two contributions at 547 cm^{-1} and 615 cm^{-1} (see Fig. 11). The component at 547 cm^{-1} can be assigned to an extrinsic defect mode induced by oxygen vacancies that can be increased in case of the substitution of Ce^{4+} by lower valence cations in a solid solution. This phenomenon has been observed for various dopants [48,49,51–53], as well as for Ni^{2+} [54–56].

This catalyst precursor thus shows both intrinsic and extrinsic oxygen vacancies although it has been calcined. This is a good indication of strong interaction between Ni and Ce species although the typical shift of the ν_s(Ce—O) band with Ce—Ni—O solid solution formation is not observed. The ratios of peak surfaces in respect to the main ν_s(Ce—O) peak are reported in Table 4 for both intrinsic (A_{Di}) and extrinsic (A_{De}) defect modes.

Both samples reacted at 600 °C show a slightly narrower ν_s(Ce—O) band at 465 cm^{-1}. Particles sizes can be estimated to 24 and 27 nm for the samples after CH_4 and CO_2, respectively. The relative contribution of the defect bands is strongly enhanced in both cases. In this case, both reduction and eventual substitution of Ce^{4+} by Ni^{2+} cations contribute to the generation of oxygen vacancies. The two samples show very similar spectra confirming that – at this temperature – the samples are in a more reduced state even after the CO_2 reaction step.

After reaction at 800 °C, the ν_s(Ce—O) band position is not affected by the last reacting atmosphere. The width of this band reveals a further increase of the particles size (59 and 76 nm after CH_4 and CO_2, respectively) in accordance with XRD results. The sample exposed to CH_4 in the last step shows an enhanced contribution of the defect bands again showing the partial reduction of the system. Interestingly, after exposure to CO_2 the sample recovers a Raman spectrum very similar to the one of the calcined catalysts. This is a good indication of the regeneration of the oxygen vector in these conditions.

3.3.5. *Dynamic behavior of Ni/CeO_2 in CLDRM*

A first approach on the dynamics of the periodic process within a specific cycle is proposed. Figs. 12–14 show the cumulated amount CH_4 consumed and of oxygen removed from the solid along the one-minute feed of CH_4 at 700 °C. Ideally, one mole of CH_4 consumed should remove one mole of oxygen from the solid in order to get $2H_2$ and 1 CO. Thus, 100% selectivity should be reached if the lines of CH_4 consumed and O removed overlap each other. Ideally, they would follow the black line corresponding to the cumulated amount of CH_4 fed into the reactor and therefore the maximum CH_4 possibly consumed. If the consumption of CH_4 is higher than the one of O removed, some carbon deposition is expected. On the contrary, if the oxygen removed is higher than the one of CH_4 consumed, some total oxidation of CH_4 occurs producing H_2O and CO_2 (besides or not some carbon deposition).

Fig. 12 shows such results obtained with three different catalyst amounts (50, 100 and 200 mg) at 700 °C. Except at the initial stage of the reductant step, methane is never totally consumed. With 50 mg of catalyst, the O removed curve seems to reach a maximum at approx. 55 μmols. The amount of methane consumed also reaches a maximum but near to 75 μmols. This is indicative of a limitation of the available oxygen for the reaction. With 100 mg, the overall O removed increases up to approx. 95 μmols. Methane consumption on the other hand reaches 120 μmols, thus indicating that carbon deposition occurs. With 200 mg, both curves are nearer to each other and increase evenly during the full step. Contrary to the experiments with lower amounts, the curves do not show tendencies to flatten due to the slowing down of O release or methane consumption.

It appears clearly that the reaction is limited by the amount of oxygen available. Interestingly, the process seems to slow down when the corresponding amount of oxygen needed to reduce CeO_2 to Ce_6O_{11} is reached (42, 84, 168 μmols for 50, 100 and 120 mg, respectively).

At 750 °C (Fig. 13), a similar trend can be observed. In this case the maximum values reach, naturally, higher values than at 700 °C. A deeper reduction of the solid is thus possible, well beyond the nominal Ce_6O_{11} composition. It can nevertheless be noted that

for both 50 and 100 mg experiments the curves of methane consumption and O removal tend to separate when this composition is reached.

These results suggest that the reduction of CeO_2 to Ce_6O_{11} would be responsible for the rapid and selective conversion of CH_4 to syngas, whereas more reduced ceria would be less reactive in terms of oxygen supply and thus lead to coke formation. Such consideration would be in accordance with the thermodynamic calculations mentioned in Section 3.1.

Nevertheless, XRD analysis of the catalysts after stopping the reaction after the reductant or oxidant steps, both at 600 and 800 °C did not reveal the presence of a Ce_6O_{11} phase in any case (Fig. 9). Thus, the actual phase transition to Ce_6O_{11} does not occur even when the corresponding nominal $CeO_{1.83}$ composition is reached or even passed.

Fig. 14 shows the methane consumption and O removal during the reductant step using samples with different Ni loadings (2, 8.8 and 38.5 wt.%). For 2 wt.%Ni, the curve of O removal is above the one of CH_4 consumption, meaning that more oxygen is available in the solid than that necessary to selectively oxidize the CH_4 which it is capable to activate. Going to the other extreme, high loading of 38.5 wt% of Ni considerably increases the amount of methane consumed as expected. On the other hand, the amount of oxygen consumed remains very similar to that of the 2 wt% loading. Most interestingly, the intermediate loading of 8.8 wt% shows an effect of Ni on both the surface activation of CH_4 and that of oxygen supply by the solid. This could also be explained by the presence of Ni species in strong interaction with Ce species with the eventual formation – in the intermediate composition range – of a Ce—Ni—O solid solution in which Ni^{2+} species promote the oxygen mobility, and thus availability for DRM, of ceria. Indeed, such solid solutions are known for $Ce_{1-x}Ni_xO_y$ with $x < 0.5$ [e.g. 37,57–59]. High loadings (38.5 wt% Ni, $x = 1.86$) would be prejudicial as independent phases can be created, forming majorly separated oxides such as NiO and CeO_2 during calcination. This NiO may lead to total oxidation during the first chemical looping cycles but then would remain in reduced state and contribute essentially to methane activation. On the contrary, a too low% of Ni (2 wt%, $x = 0.06$) can create a Ce—Ni—O

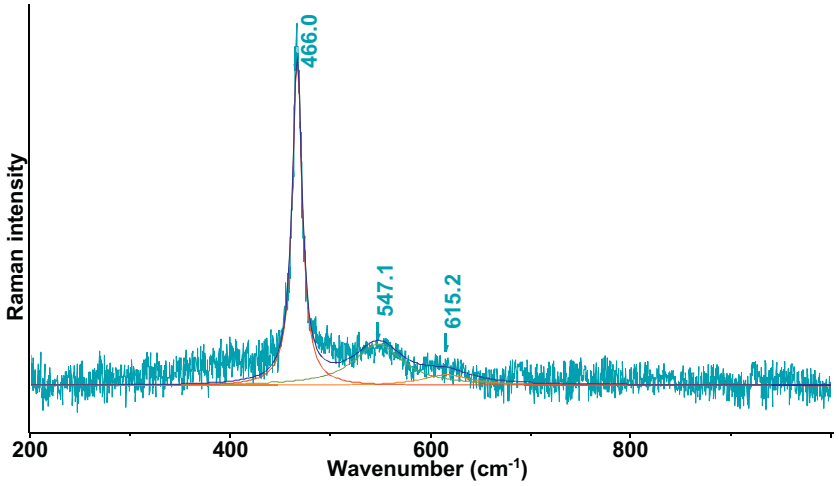

Fig. 11. Raman spectrum decomposition for Ni(9.5)/CeO_2 (800 °C, after CH_4).

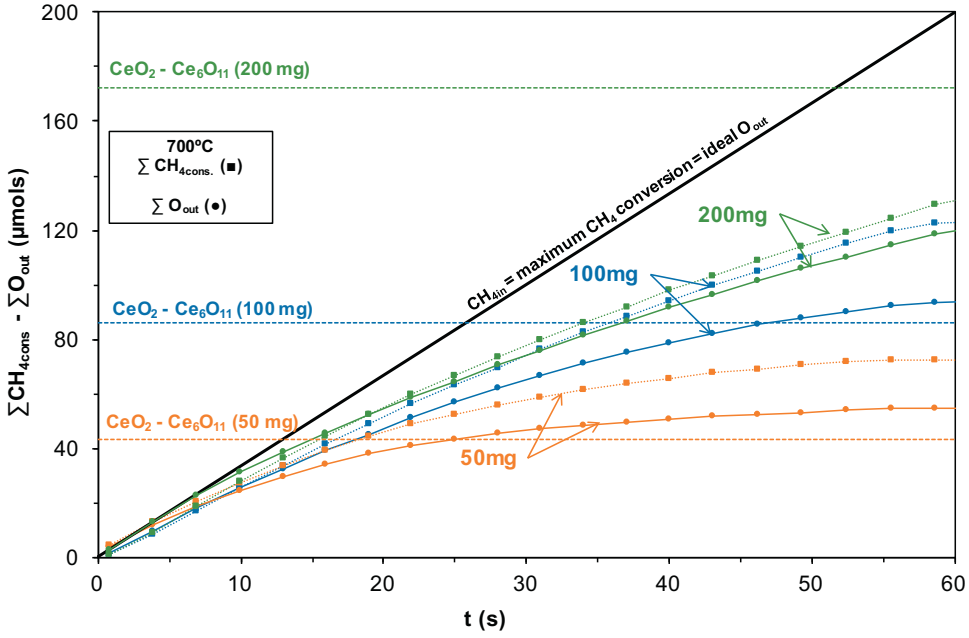

Fig. 12. O removed (●) and CH_4 consumed (■) at 700 °C on Ni(8.8)/CeO_2 with $[CH_4]_0 = 5\%$ and after 11 cycles working in periodic.

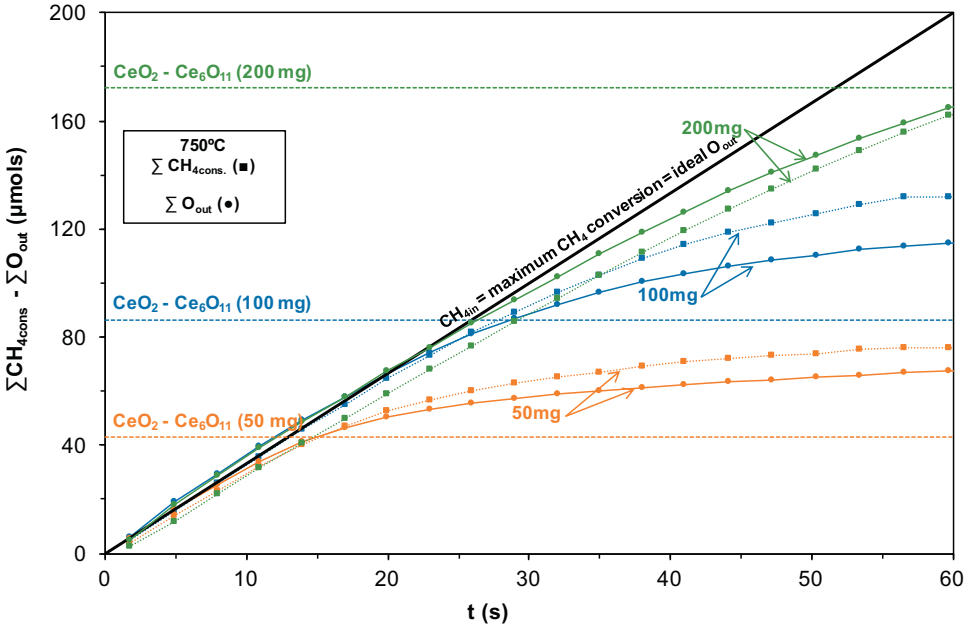

Fig. 13. O removed (●) and CH_4 consumed (■) at 750 °C on Ni(8.8)/CeO_2 with $[CH_4]_0$ = 5% and after 11 cycles working in periodic.

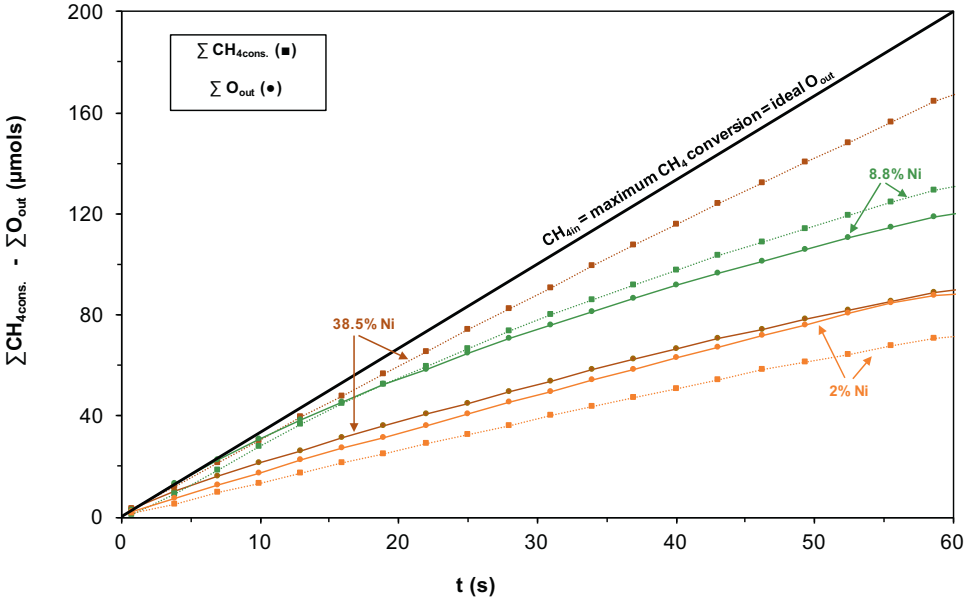

Fig. 14. O removed (●) and CH_4 consumed (■) at 700 °C on Ni(x)/CeO_2 (200 mg) with $[CH_4]_0$ = 5% and after 11 cycles working in periodic.

solid solution but not in the optimum range (not enough oxygen vacancies). However, the 9–10 wt% loading of Ni (x = 0.28–0.35) can create a solid solution near to the optimum on the studied series.

Characterization of the various solids did not reveal the presence of such solid solution. Nevertheless, both XPS and Raman scattering suggest the presence of Ni^{2+} species in strong interaction with Ce species. It can therefore be supposed that such species play an important role on the oxygen mobility in the system either in the bulk of the support or, more probably, at its surface. In this respect Ni loading, and thus distribution of these species at the surface is a crucial parameter for the optimization of such process.

4. Conclusions

The principle of periodic dry reforming of methane has been successfully demonstrated using a solid based on particles of nickel (Ni) supported on cerium dioxide (CeO_2). The support reacts as an oxygen vector by reduction and oxidation under CH_4 and CO_2 respectively. The metal is necessary to provide the good activation of methane, leading to high conversions. Bulk metallic nickel is not oxidized back to the original oxide state in presence of CO_2 under the working conditions, which is also corroborated with the thermodynamic calculations, whereas surface species may be oxidized by CO_2. In such conditions, the selectivity coming from the oxidation of methane is practically ideal towards syngas, on the contrary to when the catalyst is re-oxidized by oxygen. In addition, the main differences from other studies made in the literature are the high selectivity towards H_2/CO without a high production of H_2O with Ni/CeO_2 instead of Fe-CeO_2 formulations and the ease of the synthesis technique. Impregnation method, the most practical one for the industry, has shown promising performances for this process. Results also showed that carbon formed during exposure

to methane can be fully removed during the re-oxidation by CO_2. This allows to avoid carbon accumulation and deactivation.

From the dynamic study and the characterization of catalysts, it has been shown that Ni species play two essential roles. First, they contribute to the activation of the reactants as expected. Second, Ni also has an important role on the rate of oxygen supply from the solid, especially in the intermediate loading showing an important synergetic effect that does not appear at very low and very high loadings. This could be linked to the strong interaction of part of the surface nickel species with cerium species, and a promotion of oxygen mobility from the support to active Ni particle and backwards.

Obviously, other important aspects regarding the reactivity of such systems need to be studied such as, i.e., effect of reactant and in particular methane partial pressures or the re-oxidation process of both the oxide and of carbon. Nevertheless, this work opens the path to further optimization, in particular by:

- The control of the amount and the nature of the metallic phase, see mixed metals phase to optimize the activation of CH_4 and CO_2.
- The control of the oxygen available to react in the oxygen carrier modifying the nature of the support (oxides, mixed oxides...)

Acknowledgments

The Fonds Européen de Développement Régional (FEDER), CNRS, Région Hauts-de-France and Ministère de l'Education Nationale de l'Enseignement Supérieur et de la Recherche are acknowledged for funding of XPS/LEIS/ToF-SIMS spectrometers within the Pôle Régional d'Analyses de Surface and XRD instruments. JGC and TK are grateful to Univ. Lille and Région Hauts-de-France for providing financial support. The authors would like to thank Ms. L. Burylo (for XRD), Mr. O. Gardoll (for TPR), and Ms. M. Trentesaux (for XPS) from Unité de Catalyse et Chimie du Solide.

Appendix A. Supplementary data

Supplementary data associated with this article can be found, in the online version, at http://dx.doi.org/10.1016/j.apcatb.2017.04.048.

References

[1] J.W. Thybaut, G.B. Marin, C. Mirodatos, Y. Schuurman, A.C. van Veen, V.A. Sadykov, H. Pennemann, R. Bellinghausen, L. Mleczko, A novel technology for natural gas conversion by means of integrated oxidative coupling and dry reforming of methane, Chem. Ing. Tech. 86 (2014) 1855–1870.
[2] Y.T. Shah, T.H. Gardner, Dry reforming of hydrocarbon feedstocks, Catal. Rev.—Sci. Eng. 56 (4) (2014) 476–536.
[3] H. Liu, C. Guan, X. Li, L. Cheng, J. Zhao, N. Xue, W. Ding, The key points of highly stable catalysts for methane reforming with carbon dioxide, Geophys. Res. 110 (2005) C09S05.
[4] A.M. Amin, E. Croiset, W. Epling, Review of methane catalytic cracking for hydrogen production, Int. J. Hydrogen Energy 36 (2011) 2904–2935.
[5] P. Lahijani, Z.A. Zainal, M. Mohammadi, A.R. Mohamed, Conversion of the greenhouse gas CO_2 to the fuel gas CO via the Boudouard reaction: a review, Renew. Sustain. Energy 41 (2015) 615–632.
[6] L.A. Gould, L.B. Evans, H. Kurihara, Optimal control of fluid catalytic cracking processes, Automatica 6 (1970) 695–703.
[7] A. Corma, L. Sauvanaud, FCC testing at bench scale: new units new processes, new feeds, Catal. Today 218–219 (2013) 107–114.
[8] J. Adanez, A. Abad, F. Garcia-Labiano, P. Gayan, L.F. de Diego, Progress in chemical-looping combustion and reforming technologies, Prog. Energy Combust. 38 (2012) 215–282.
[9] M.M. Hossain, H.I. de Lasa, Chemical-looping combustion (CLC) for inherent CO_2 separations—a review, Chem. Eng. Sci. 63 (2008) 4433–4451.
[10] R.M. Contractor, H.S. Horowitz, G.M. Sisler, E. Bordes, The effects of steam on n-butane oxidation over VPO as studied in a riser reactor, Catal. Today 37 (1997) 51–57.
[11] J.R. Fernandez, A. Vega, F.V. Diez, Partial oxidation of n-butane to maleic anhydride over VPO in a simulated circulating fluidized bed reactor, Appl. Catal. A: Gen. 376 (2010) 76–82.
[12] V. Sadykov, V. Rogova, E. Ermakova, D. Arendarsky, N. Mezentseva, G. Alikina, N. Sazonova, A. Bobin, S. Pavlova, Y. Schuurman, C. Mirodatos, Mechanism of CH_4 dry reforming by pulse microcalorimetry: metal nanoparticles on perovskite/fluorite supports with high oxygen mobility, Thermochim. Acta 567 (2013) 27–34.
[13] K. Otsuka, Y. Wang, E. Sunada, I. Yamanaka, Direct partial oxidation of methane to synthesis gas by cerium oxide, J. Catal. 175 (1998) 152–160.
[14] S. Bhavsar, M. Najera, G. Veser, Chemical looping dry reforming as novel, intensified process for CO_2 activation, Chem. Eng. Technol. 35 (2012) 1281–1290.
[15] S. Bhavsar, M. Najera, R. Solunke, G. Veser, Chemical looping: to combustion and beyond, Catal. Today 228 (2014) 96–105.
[16] S. Bhavsar, G. Veser, Reducible supports for Ni-based oxygen carriers in chemical looping combustion, Energy Fuel 27 (2013) 2073–2084.
[17] S. Bhavsar, G. Veser, Chemical looping beyond combustion: production of synthesis gas via chemical looping partial oxidation of methane, RSC Adv. 4 (2014) 47254–47267.
[18] X. Zhu, K. Li, Y. Wei, H. Wang, L. Sun, Chemical-looping steam methane reforming over a CeO_2-Fe_2O_3 oxygen carrier: evolution of its structure and reducibility, Energy Fuels 28 (2014) 754–760.
[19] V. Galvita, H. Poelman, C. Detavernier, G. Marin, Catalyst-assisted chemical looping for CO_2 conversion to CO, Appl. Catal. B: Environ. 164 (2015) 184–191.
[20] S. Assabumrungrat, S. Charoenseri, N. Laosiripojana, W. Kiatkittipong, P. Praserthdam, Effect of oxygen addition on catalytic performance of Ni/SiO_2-MgO toward carbon dioxide reforming of methane under periodic operation, Int. J. Hydrogen Energy 34 (2009) 6211–6220.
[21] M. Tang, L. Xu, M. Fan, Progress in oxygen carrier development of methane-based chemical-looping reforming: a review, Appl. Energy 151 (2015) 143–156.
[22] C. Li, Y. Sakata, T. Arai, K. Domen, K.I. Maruya, T. Onishi, Carbon monoxide and carbon dioxide adsorption on cerium oxide studied by fourier-transform infrared spectroscopy, J. Chem. Soc. Faraday Trans. 1 (85) (1989) 929–943.
[23] O. Demoulin, M. Navez, J.L. Mugabo, P. Ruiz, The oxidizing role of CO_2 at mild temperature on ceria-based catalysts, Appl. Catal. B 70 (2007) 284–293.
[24] F. Dury, E.M. Gaigneaux, P. Ruiz, The active role of CO_2 at low temperature in oxidation processes: the case of the oxidative dehydrogenation of propane on $NiMoO_4$ catalysts, Appl. Catal. A: Gen. 242 (2003) 187–203.
[25] T. Jin, T. Okuhara, G.J. Mains, J.M. White, Temperature-programmed desorption of CO and CO_2 from Pt/CeO_2. An important role for lattice oxygen in CO oxidation, J. Phys. Chem. 91 (1987) 3310–3315.
[26] S. Sharma, S. Hilaire, J.M. Vohs, R.J. Gorte, H.W. Jen, Evidence for oxidation of ceria by CO_2, J. Catal. 190 (2000), 199–120.
[27] T. Staudt, Y. Lykhach, N. Tsud, T. Skala, K.C. Prince, V. Matolin, J. Libuda, Ceria reoxidation by CO_2: a model study, J. Catal. 275 (2010) 181–185.
[28] C. Bale, E. Bélisle, P. Chartrand, S. Decterov, G. Eriksson, K. Hack, I. Jung, Y. Kang, J. Melançon, A. Pelton, C. Robelin, S. Petersen, FactSage thermochemical software and databases— recent developments, Calphad 33 (2009) 295–311 [Online] [Accessed 2013–2015] www.factsage.com.
[29] Y.H. Taufiq-Yap, Sudarno, U. Rashid, Z. Zainal, CeO_2-SiO_2 supported nickel catalysts for dry reforming of methane toward syngas production, Appl. Catal. A 468 (2013) 359–369.
[30] L. Jalowiecki-Duhamel, H. Zarrou, A. D'Huysser, Hydrogen production at low temperature from methane on cerium and nickel based mixed oxides, Int. J. Hydrogen 33 (2008) 5527–5534.
[31] W. Fang, C. Pirez, S. Paul, M. Capron, H. Jobic, F. Dumeignil, L. Jalowiecki-Duhamel, Room temperature hydrogen production from ethanol over $CeNi_xH_zO_y$ nano-oxyhydride catalysts, ChemCatChem 5 (2013) 2207–2216.
[32] V. Galvita, K. Sundmacher, Hydrogen production from methane by steam reforming in a periodically operated two-layer catalytic reactor, Appl. Catal. A: Gen. 289 (2005) 121–127.
[33] F. Esch, S. Fabris, L. Zhou, T. Montini, C. Africh, P. Fornasiero, G. Comelli, R. Rosei, Electron localization determines defect formation on ceria substrates, Science (2005) 752–755.
[34] L. Liu, C. Zhao, Y. Li, Spontaneous dissociation of CO_2 to CO on defective surface of Cu(I)/TiO_{2-x} nanoparticles at room temperature, J. Phys. Chem. C 116 (2012) 7904–7912.
[35] X. Chang, T. Wang, J. Gong, CO_2 photo-reduction: insights into CO_2 activation and reaction on surfaces of photocatalysts, Energy Environ. Sci. 9 (2016) 2177–2196.
[36] E. Bêche, P. Charvin, D. Perarnau, S. Abanades, G. Flamant, Ce 3d XPS investigation of cerium oxides and mixed cerium oxide ($Ce_xTi_yO_z$), Surf. Interface Anal. 40 (2008) 264–267.
[37] A. Ponchel, A. D'Huysser, C. Lamonier, L. Jalowiecki-Duhamel, $CeNi_xO_y$ and $CeAl_zNi_xO_y$ solids studied by electron microscopy, XRD, XPS and depth sputtering techniques, Phys. Chem. Chem. Phys. 2 (2000) 303–312.
[38] A.P. Grosvenor, M.C. Biesinger, R.St.C. Smart, N.S. McIntyre, New interpretations of XPS spectra of nickel metal and oxides, Surf. Sci. 600 (2006) 1771–1779.
[39] G. Poncelet, M.A. Centeno, R. Molina, Characterization of reduced α-alumina-supported nickel catalysts by spectroscopic and chemisorption measurements, Appl. Catal. A: Gen. 288 (2005) 232–242.

[40] W. Shan, M. Fleys, F. Lapicque, D. Swierczynski, A. Kiennemann, Y. Simon, P.-M. Marquaire, Syngas production from partial oxidation of methane over $Ce_{1-X}Ni_XO_Y$ catalysts prepared by complexation-combustion method, Appl. Catal. A: Gen. 311 (2006) 24–33.
[41] J. Wang, M. Shen, J. Wang, M. Yang, W. Wang, J. Ma, L. Jia, Effects of Ni-doping of ceria-based materials on their micro-structures and dynamic oxygen storage and release behaviors, Catal. Lett. 140 (2010) 38–48.
[42] D. Kong, J. Zhu, K.H. Ernst, Low-temperature dissociation of CO_2 on a $Ni/CeO_2(111)/Ru(0001)$ model catalyst, J. Phys. Chem. C 120 (2016) 5980–5987.
[43] A. Trovarelli, Structural properties and nonstoichiometric behavior of CeO_2, in: A. Trovarelli (Ed.), Catalysis by Ceria and Related Materials, Imperial College Press, London, UK, 2002, p. 15.
[44] I. Kosacki, T. Suzuki, H.U. Anderson, P. Colomban, Raman scattering and lattice defects in nanocrystalline CeO_2 thin films, Solid State Ionics 149 (2002) 99–105.
[45] J.E. Spanier, R.D. Robinson, F. Zhang, S.W. Chan, I. Herman, Size-dependent properties of CeO_{2-y} nanoparticles as studied by Raman scattering, Phys. Rev. B 64 (2001) 2454071–2454078.
[46] M.D. Hernaíndez-Alonso, A.B. Hungria, A. Martinez-Arias, J.M. Coronado, J.C. Conesa, J. Soria, M. Fernandez-Garcia, Confinement effects in quasi-stoichiometric CeO_2 nanoparticles, Phys. Chem. Chem. Phys. 6 (2004) 3524–3529.
[47] F. Zhang, S.W. Chan, J.E. Spanier, E. Apak, Q. Jin, R.D. Robinson, I.P. Herman, Cerium oxide nanoparticles: size-selective formation and structure analysis, Appl. Phys. Lett. 80 (2002) 127–129.
[48] J.R. McBride, K.C. Hass, B.D. Poindexter, W.H. Weber, Raman and x-ray studies of $Ce_{1-x}RE_xO_{2-y}$, where RE = La, Pr, Nd, Eu, Gd, and Tb, J. Appl. Phys. 76 (1994) 2435.
[49] N. Paunovicí, Z. Dohčevicí-Mitrovicí, R. Scurtu, S. Aškrabicí, M. Prekajski, B. Matovicí, Z.V. Popovicí, Suppression of inherent ferromagnetism in Pr-doped CeO_2 nanocrystals, Nanoscale 4 (2012) 5469–5476.
[50] C.G. Rotaru, G. Postole, M. Florea, F. Matei-Rutkovska, V.I. Pârvulescu, P. Gelin, Dry reforming of methane on ceria prepared by modified precipitation route, App. Catal. A: Gen. 494 (2015) 29–40.
[51] M. Daniel, S. Loridant, Probing reoxidation sites by in situ Raman spectroscopy: differences between reduced CeO_2 and Pt/CeO_2, J. Raman Spectrosc. 43 (2012) 1312–1319.
[52] A. Mineshige, T. Taji, Y. Moroi, M. Kobune, S. Fujii, N. Nishi, M. Inaba, Z. Ogumi, Oxygen chemical potential variation in ceria-based solid oxide fuel cells determined by Raman spectroscopy, Solid State Ionics 135 (2000) 481–485.
[53] G. Li, R.L. Smith Jr., H. Inomata, Synthesis of nanoscale $Ce_{1-x}Fe_xO_2$ solid solutions via a low-temperature approach, J. Am. Chem. Soc. 123 (2001) 11091–11092.
[54] Y.M. Liu, J.C. Wang, M. Chen, J. Xu, Y. Cao, H.Y. He, K.N. Fan, Highly selective Ce–Ni–O catalysts for efficient low temperature oxidative dehydrogenation of propane, Catal. Lett. 130 (2009) 350–354.
[55] X. Du, D. Zhang, L. Shi, R. Gao, J. Zhang, Morphology dependence of catalytic properties of Ni/CeO_2 nanostructures for carbon dioxide reforming of methane, J. Phys. Chem. C 116 (2012) 10009–10016.
[56] Sk. Mahammadunnisa, P. Manoj Kumar Reddy, N. Lingaiah, Ch. Subrahmanyam, $NiO/Ce_{1-x}Ni_xO_{2-\delta}$ as an alternative to noble metal catalysts for CO oxidation, Catal. Sci. Technol. 3 (2013) 730–736.
[57] G. Wrobel, M.P. Sohier, A. D'Huysser, J.P. Bonnelle, J.P. Marcq, Hydrogenation catalysts based on nickel and rare earth oxides: part II: XRD, electron microscopy and XPS studies of the cerium-nickel-oxygen-hydrogen system, Appl. Catal. A: Gen. 101 (1993) 73–93.
[58] G. Wrobel, C. Lamonier, A. Bennani, A. D'Huysser, A. Aboukaïs, Effect of incorporation of copper or nickel on hydrogen storage in ceria, J. Chem. Soc. Faraday Trans. 92 (1996) 2001–2009.
[59] C. Lamonier, A. Ponchel, A. D'Huysser, L. Jalowiecki-Duhamel, Studies of the cerium-metal-oxygen-hydrogen system (metal = Cu, Ni), Catal. Today 50 (1999) 247–259.